Journal of Solid State Chemistry 184 (2011) 2571–2579

Contents lists available at ScienceDirect

Journal of Solid State Chemistry

journal homepage: www.elsevier.com/locate/jssc

Rare earth (Eu^{3+}, Tb^{3+}) mesoporous hybrids with calix[4]arene derivative covalently linking MCM-41: Physical characterization and photoluminescence property

Ya-Juan Li, Bing Yan*, Li Wang

Department of Chemistry, Tongji University, Siping Road 1239, Shanghai 200092, China

ARTICLE INFO

Article history:
Received 19 April 2011
Received in revised form
20 July 2011
Accepted 24 July 2011
Available online 2 August 2011

Keywords:
Mesoporous hybrids
Calix[4]arene derivative as covalent linkage
Rare earth ions
Luminescence

ABSTRACT

MCM-41 mesoporous silica has been functionalized with two kinds of macrocylic calixarene derivatives Calix[4] and Calix[4]Br (Calix[4]=P-*tert*-butylcalix[4]arene, Calix[4]Br=5.11,17.23-tetra-*tert*-butyl-25.27-bihydroxy-26.28-bibromopropoxycalix[4]arene) through condensation approach of tetraethoxysilane (TEOS) in the presence of the cetyltrimethylammonium bromide (CTAB) surfactant as a template. Novel organic–inorganic mesoporous luminescent hybrid containing RE^{3+} (Eu^{3+}, Tb^{3+}) complexes covalently attached to the functionalized ordered mesoporous MCM-41, which are designated as *RE*-Calix[4]-MCM-41 and *RE*-Calix[4]Br-MCM-41, respectively, are obtained by sol–gel process. It is found that they all have high surface area, uniform in the mesostructure and good crystallinity. Measurement of the photoluminescence properties show the mesoporous material covalently bonded Tb^{3+} complexes (Tb-Calix[4]-MCM-41 and Tb-Calix[4]Br-MCM-41) exhibit the stronger characteristic emission of Tb^{3+} and longer lifetime than the corresponding Eu-containing materials Eu-Calix[4]-MCM-41 and Eu-Calix[4]Br-MCM-41 due to the triplet state energy of modified organic ligands Calix[4]-Si and Calix[4]Br–Si match with the emissive energy level of Tb^{3+} very well.

1. Introduction

Calixarenes, a versatile class of macrocyclic compounds possessing soft π-donor cavities composed of benzene rings and hard oxygen cavities constructed on the hydroxyl lower rim, have gained an important place in host-guest chemistry because of their ability to form complexes with ions and neutral molecules [1–5]. In particular functionalization of the lower rim of calix[4]-arenes with suitable binding groups has produced a series of powerful cation receptors whose efficiency and selectivity is related to the calixarene ring size and conformation. The covalent attachment of calixarene, by suitable bridges, to luminescent metal ions can result in systems capable of exhibiting novel and unusual photophysical properties [3]. A particularly interesting class of luminescent metal ions is the rare earth family because they show long-lived and strong narrow-width emission bands, which cover a spectral range from the near-ultraviolet to the visible and the near-infrared region and high luminescence quantum efficiency [4]. However, it is difficult to generate efficient luminescence by direct excitation of the rare earth ion, because of the low extinction coefficients of the Laporte-forbidden *f*–*f* transitions [6]. To overcome this difficult, the rare earth ions are usually chelated with organic ligands that have broad, intense absorption bands. The metal-centered luminescence originates from the intramolecular energy transfer through the excited state of the ligand to the emitting level of the rare earth ion. This is the so-called "antenna effect" [7,8]. Most of the investigations in the field of luminescent rare earth complexes have been devoted to Eu^{3+} and Tb^{3+} compounds [9,10], which emit in the visible spectral region and are used as sensors and as luminescent labels in fluoroimmunoassays and time-resolved microscopy [3,11]. However, there exist some restrictions for the practical application of these complexes, essentially owing to their poor thermal stabilities under high temperature or moisture conditions and low mechanical strength. In order to overcome these drawbacks, rare earth complexes should be incorporated into some stable inorganic matrix, for example, polymers [12], liquid crystal [13], or silica-based materials [14]. The conventional process (called physical doping), embedding the luminescent centers into inorganic matrices, could not avoid many problems, such as inhomogeneous distribution of the complexes, limitation of the concentration or phase separation, since the complex and inorganic matrices are mixed by weak interactions (hydrogen bonding, van der Waals force, or static effect) [15]. So another kind of hybrid appeared, which belongs to the molecular-based composite material and could realize the

* Corresponding author. Fax: +86 21 65982287.
E-mail address: byan@tongji.edu.cn (B. Yan).

0022-4596/$ - see front matter © 2011 Elsevier Inc. All rights reserved.
doi:10.1016/j.jssc.2011.07.040

possibility of tailoring the complementary properties of novel multifunctional materials through the combination with different components mixed by chemical covalent bonds (caller chemical bonding) [16,17].

Mesoporous silica materials are attractive hosts for the preparation and investigation of inorganic–organic hybrid materials, since they offer many novel and unique properties, such as the rigidity, photostability, and well-defined hydrophilic/hydrophobic phase separation [18–22]. Mesoporous materials M41S have long been the hot research subject due to their unique surface and uniform pore structure since they are synthesized in 1992. MCM-41, one member of the M41S family, possesses regularly hexagonal arrays of mesopores, changeable pore diameter between 1.5 and 30 nm and tailorable interior surfaces [23]. In addition, there is a large number of hydroxyl in MCM-41, which provides necessary qualification for the modification of inner face and self-assembly of huge guest molecules, namely, providing outstanding hosts for self-aggregation chemistry. The modified mesoporous SBA-15-typed materials with the different calix[4]arene derivatives have been reported [24]. These properties together with the thermal and mechanical stabilities make the MCM-41 material ideal candidate as a host for the rare earth complexes. Recently, Zhang et al. [25,26] and our group [27,28] have reported the synthesis of MCM-41 mesoporous materials covalently bonded with rare earth complexes. It is shown that the promising visible-luminescent properties can be obtained by linking the rare earth complexes to the mesoporous materials. However, the synthesis and luminescence properties of MCM-41 mesoporous materials covalently bonded with rare earth complexes by the modified calixarene, to the best of our knowledge, have not been reported in by other group up till now.

Taking into account the above we here present the systematic and comparative study of the MCM-41 mesoporous silica covalently bonded with rare earth complexes functionalized by two kinds of calixarene designated as *RE*-Calix[4]-MCM-41 and *RE*-Calix[4]Br-MCM-41 (*RE*=Eu, Tb; Calix[4]=P-*tert*-butylcalix[4]arene, Calix[4]Br =5.11,17.23-tera-*tert*-butyl-25.27-bihydroxy-26.28-bibromopropoxycalix[4]arene; Calix[4]-MCM-41 and Calix[4]Br-MCM-41 denote Calix[4]-functionalized MCM-41 mesoporous material and Calix[4]Br-functionalized MCM-41 mesoporous material, respectively). Full characterization and detail studies of all these synthesized materials are investigated and compared.

2. Experimental

2.1. Chemicals

Tetraethoxysilane (TEOS, Aldrich), 3-(triethoxysilyl)propyl isocyanate (TEPIC, Lancaster), Cetyltrimethylammonium bromide (CTAB), fuming nitric acid (HNO_3), and ethanol (EtOH) are used as received. The solvents pyridine and tetrahydrofuran (THF) are used after desiccation with anhydrous calcium chloride. $RE(NO_3)_3$ (*RE*=Eu, Tb) ethanol solution (EtOH) are prepared by dissolving their respective oxides (Eu_2O_3 and Tb_4O_7) in concentrated nitric acid (HNO_3). P-*tert*-butylcalix[4]arene (Calix[4] as the abbreviation in this paper), and p-*tert*-butylcalix[4] arene derivative (5.11,17.23-tera-*tert*-butyl-25.27-bihydroxy-26.28-bibromopropoxycalix[4]arene) (Calix[4]Br) are synthesized according to Ref. [2].

2.2. Synthesis

2.2.1. Synthesis of macrocylic precursor Calix[4]-Si with Si–O covalent bonds

The modified precursor Calix[4]-Si is synthesized according to the procedure in the literature [29]: Typically, Calix[4] (1 mmol, 0.424 g) is first dissolved in 20 mL pyridine solvent. Then, 1 mmol (0.247 g) of TEPIC is added dropwise into the solution with stirring. The mixture is heated at 60 °C in a covered flask for approximately 12 h under nitrogen atmosphere. The coating liquid is concentrated to remove the solvent using a rotary vacuum evaporator, and a yellow oil sample is obtained and dried in a vacuum, and then recrystallized by toluene with the yield of 68%. Calix[4]-Si ($C_{54}H_{77}NSiO_8$) IR: −CONH-1647 cm^{-1}, $-(CH_2)_3-$ 2971 cm^{-1}, Si–O 1079 cm^{-1}. ^1H NMR ($CDCl_3$, 500 MHz): δ 0.65 (2H, t), 1.22 (9H, t), 1.23 (36H, m, $C(CH_3)_3$), 1.65 (2H, m), 3.16 (2H, m), 3.83 (6H, m), 4.27 (8H, m, Ar–CH_2–Ar), 4.53 (1H, s, NH), 7.21 (8H, s, Ar–H), 10.22 (3H, s, Ar–OH). ^{13}CNMR data ($CDCl_3$, 500 MHz): δ7.57 (C_{13}), 17.34 (C_{12}), 17.47 (C_{11}), 18.28 (C_{10}), 18.44 ($CH_3(OCH_3)$), 21.45 (C_9), 25.13 (C_8), 45.40 (C_7), 58.49 ($CH_2(OCH_3)$), 70.59 (C_6), 125.30 (C_5), 128.23 (C_{2-4}), 129.04 (C_1).

2.2.2. Synthesis of macrocylic precursor Calix[4]Br–Si with Si–O covalent bonds

Calix[4]-Br (1 mmol, 0.89 g) is dissolved in 20 mL tetrahydrofuran solvent (THF) and after complete dissolution 2.0 mmol (0.495 g) of TEPIC is dropwise added into the solution with stirring. The mixture is heated at 60 °C in a covered flask for approximately 12 h at the nitrogen atmosphere. The coating liquid is concentrated to remove the solvent using a rotary vacuum evaporator and the transparent viscous liquid sample is obtained. Then the liquid sample is dissolved in absolute ethanol, and 20 mL of hexane is added into the solution to precipitate, subsequently, the solution is filtrated. The above procedures of dissolution and filtration are repeated three times. At last the pure white powder is obtained and dried in a vacuum with the yield of 72%. Calix[4]Br–Si ($C_{70}H_{108}O_{12}Br_2N_2Si_2$) IR: −CONH-1705 cm^{-1}, $-(CH_2)_3$-2957 cm^{-1}, Si–O 1072 cm^{-1}. ^1H NMR ($CDCl_3$, 500 MHz): δ0.67 (4H, t), 0.84, 1.02 (36H, s, $C(CH_3)_3$), 1.25 (18H, t), 1.71 (4H, m), 2.56 (m, 4H), 3.31, 3.34 (4H, t), 3.84 (12H, m), 4.02, 4.12 (4H, t), 4.25, 4.27 (8H, s, Ar–CH_2–Ar), 4.42 (2H, t, NH), 7.09, 6.91 (8H, s, Ar–H). ^{13}CNMR data ($CDCl_3$, 500 MHz): δ7.50 (C_{18}), 14.56 ($CH_3(OCH_3)$), 21.98 (C_{17}), 24.05 (C_{16}), 23.28 (C_{15}), 30.29 (($CH_2(OCH_3)$)), 30.98 (C_{14}), 31.61 (C_{13}), 31.84 (C_{12}), 42.93 (C_{11}), 125.18 (C_{10}), 125.66 (C_9), 127.55 (C_8), 132.76 (C_7), 141.74 (C_6), 147.31 (C_5), 149.16 (C_4), 150.51 (C_3), 158.85 (C_{2-4}), 177.97 (C_1).

2.2.3. Synthesis of Calix[4]-functionlized MCM-41 mesoporous material (Calix[4]-MCM-41)

In a typical procedure, 1.65 g of CTAB is dissolved in concentrated $NH_3 \cdot H_2O$ (18 mL), to which deionized water (39 mL), TEOS and Calix[4]-Si are added into the above solution, leading to a composition with a molar ratio of 0.02 Calix[4]-Si: 0.98 TEOS: 0.139 CTAB: 3.76 $NH_3 \cdot H_2O$: 66.57H_2O. The mixture is stirred at room temperature for 24 h and transferred into a Teflon bottle sealed in an autoclave, which is then heated at 100 °C for 48h. Then the solid product is filtered, washed thoroughly with deionized water, and dried at 60 °C. Removal of surfactant CTAB is conducted by Soxhlet extraction with ethanol under reflux for 2 days to give the sample denoted as Calix[4]-MCM-41 (see Scheme 1).

2.2.4. Synthesis of Calix[4]Br-functionlized MCM-41 mesoporous material (Calix[4]Br-MCM-41)

The synthesis procedure of Calix[4]Br-MCM-41 is similar to that of Calix[4]-MCM-41 except that Calix[4]-Si is replaced by Calix[4]Br–Si.

2.2.5. Synthesis of mesoporous hybrid materials RE-Calix[4]-MCM-41 (RE=Eu, Tb)

The Calix[4]-MCM-41-derived hybrid mesoporous materials containing RE^{3+} are prepared as follows: while being stirred, Calix[4]-MCM-41(0.02) is soaked in an appropriate amount of

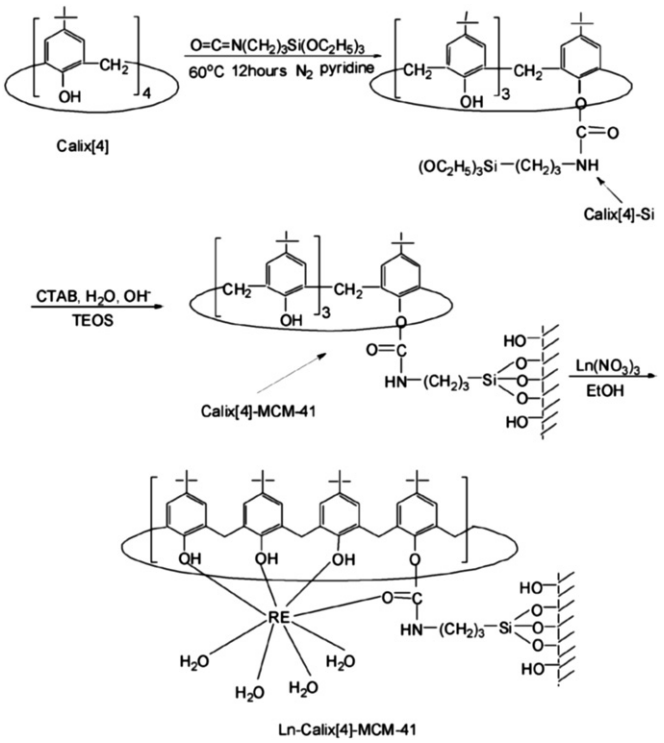

Scheme 1. Synthesis process and predicted structures of the lanthanide mesoporous hybrid materials: (A) *Ln*-Calix[4]-MCM-41.

$RE(NO_3)_3$ ethanol solution with the molar ratio of $RE(NO_3)_3$: Calix[4]-MCM-41 = 1: 1. The mixture is stirred at room temperature for 12 h followed by filtration and extensive washing with ethanol. The resulting material *RE*-Calix[4]-MCM-41 is dried at 60 °C under vacuum overnight (Scheme 1).

2.2.6. Synthesis of mesoporous hybrid materials RE-Calix[4]Br-MCM-41 (RE=Eu, Tb)

The synthesis procedure for *RE*-Calix[4]Br-MCM-41 is similar to that of *RE*-Calix[4]-MCM-41 except that the precursors Calix[4]-MCM-41 is replaced by Calix[4]Br-MCM-41 and the molar ratio of RE^{3+}: Calix[4]Br-MCM-41 being 2:1 (Scheme S1).

2.3. Physical characterization

FTIR spectra are measured within the 4000–400 cm^{-1} region on an infrared spectrophotometer with the KBr pellet technique. ^1H NMR spectra are recorded in $CDCl_3$ on a BRUKER AVANCE-500 spectrometer with tetramethylsilane (TMS) as inter reference. The ultraviolet absorption spectra are taken with an Agilent 8453 spectrophotometer. Small-angle X-ray diffraction patterns (XRD) are recorded on a Rigaku D/max-rB diffractometer equipped with a Cu anode in a 2θ range from 0.6° to 6°. Nitrogen adsorption/desorption isotherms are measured at liquid nitrogen temperature using a Nova 1000 analyzer with nitrogen. Surface areas are calculated by the Brunauer–Emmett–Teller (BET) method and pore size distributions are evaluated from the desorption branches of the nitrogen isotherms using the Barrett–Joyner–Halenda (BJH) model. Transmission electron microscope (TEM) experiments are conducted on a JEOL2011 microscopy operated at 200 kV or on a JEM-4000EX microscope operated at 400 kV. The fluorescence excitation and emission spectra are obtained by an RF-5301 spectrophotometer. Luminescence lifetime measurements are carried out on an Edinburgh FLS920 phosphorimeter using a 450 W xenon lamp as excitation source. Thermogravimetric analysis (TGA) is performed on a Netzsch STA 409C at a heating rate of 15 °C/min under nitrogen atmosphere.

3. Results and discussion

3.1. Calixarene-functionalized mesoporous silica MCM-41 (Calix[4]-MCM-41 and Calix[4]Br-MCM-41)

The presence of the calixarene ligand covalently bonded to the mesoporous MCM-41 is characterized by IR and UV absorption spectra. Fig. 1 displays the Fourier transform infrared spectra of Calix[4]Br (A), precursor Calix[4]Br–Si (B), and Calix[4]Br-functionalized mesoporous hybrid material Calix[4]Br-MCM-41 (C). In Fig. 1(A), it can be observed that the peaks at 1595 and 1480 cm^{-1} belong to the characteristic properties of benzene ring and the peaks at 1360, 1200, and 772 cm^{-1} have represented the groups $C(CH_3)_3$, Ar–O and Ar–H, respectively. The vibration of $-CH_2-$ is observed at 2960 cm^{-1} in Fig. 1(A) and it is replaced by the peaks at 2957, 2920, and 2887 cm^{-1} in Fig. 1(B), which originated from CH_2, CH_3 and ethoxy groups of TEPIC. In addition, the broad peak at 3410 cm^{-1} has indicated the existence of the associated hydroxyl group of phenol, which has disappeared and a new broad peak at 3395 cm^{-1} has emerged in Fig. 1(B) derived from the characteristic stretching vibration peak of the group NH due to the grafted reaction between the crosslinking agent TEPIC and the Calix-Br. The spectrum of Calix[4]Br–Si is dominated by ν (C-Si, 1161 cm^{-1}) and ν (Si–O, 1072 cm^{-1}) absorption bands, and the peak at 1543 cm^{-1} corresponding to the bending vibration of grafted –NH group. A new band at 1705 cm^{-1} is probably due to the stretching vibration of the –CONH– group in Calix[4]Br–Si, proving that TEPIC is successfully covalently bonded onto the ligand Calix-Br. Besides, the peaks of the isocyanate group (–N=C=O of the TESPIC molecule) around 2268 cm^{-1} are not shown in Fig. 1(B), which also suggests that TEPIC has been successfully grafted onto the –OH groups of the Calix-Br. The spectra of mesoporous hybrid material (C) indicated the formation of a Si–O–Si framework, which is evidenced by the broad bands located at 1087 cm^{-1} (ν_{as}, Si–O), 801 cm^{-1} (ν_s, Si–O), and 468 cm^{-1} (δ, Si–O–Si), which is attributed to the success of hydrolysis and copolycondensation [30]. Furthermore, the bands at 1654 and 1536 cm^{-1} originating from –CONH group of Calix[4]Br–Si, can also be observed in panel C of Fig. 1, which is consistent with the fact that the Calix[4]Br group in the framework remains intact after both hydrolysis–condensation reaction

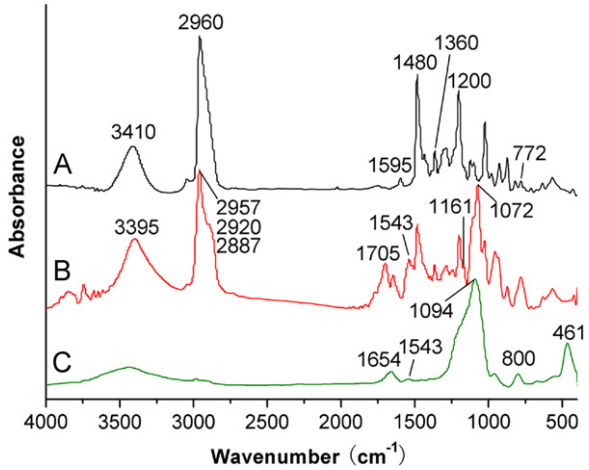

Fig. 1. FTIR spectra of the free ligand Calix[4]Br (A), precursor Calix[4]Br–Si (B), and Calix[4]Br-functionalized mesoporous hybrid material Calix[4]Br-MCM-41 (C).

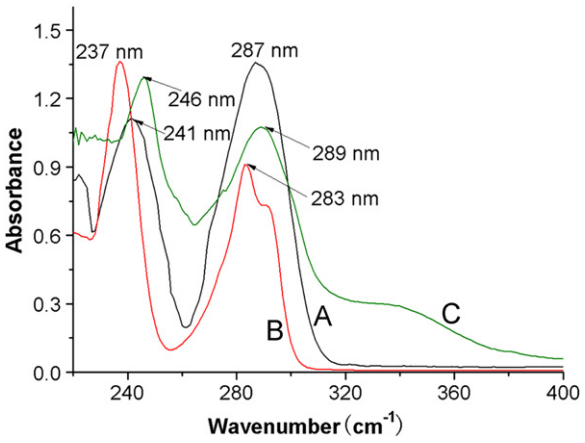

Fig. 2. Ultraviolet absorption spectra of the free ligand Calix[4]Br (A), precursor Calix[4]Br–Si (B), and Calix[4]Br-functionalized mesoporous hybrid material Calix[4]Br-MCM-41 (C).

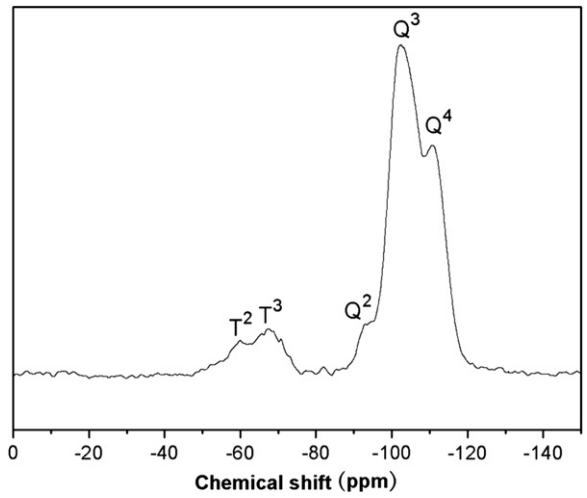

Fig. 3. ^{29}Si MAS NMR spectrum of the Calix[4]-functionalized mesoporous silica Calix[4]-MCM-41.

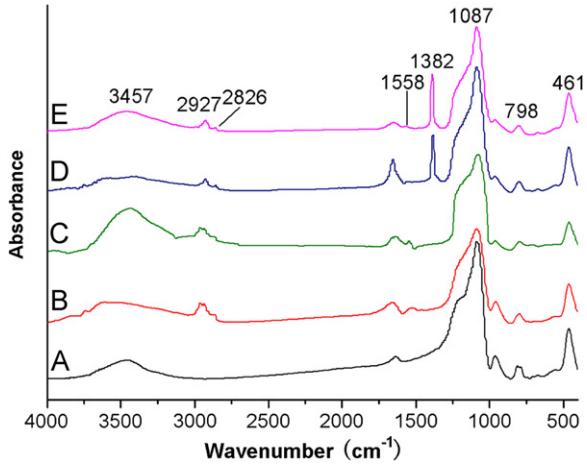

Fig. 4. FTIR spectra of MCM-41 (A), Eu-Calix[4]Br-MCM-41 (B), Tb-Calix[4]Br-MCM-41 (C), Eu-Calix[4]-MCM-41 (D), and Tb-Calix[4]-MCM-41 (E).

and the surfactant extraction procedure. Fig. S1 shows the FTIR spectra of of C[4] (A), the precursor C[4]-Si (B), and mesoporous hybrid C[4]-MCM-41 (C), which presents the similar feature as above.

The ultraviolet absorption spectra for the ligand Calix[4]Br (A), the precursor Calix[4]Br–Si (B), and Calix[4]Br-functionalized mesoporous material Calix[4]Br-MCM-41 (C) have been shown in Fig. 2. The measurement of UV–visible spectra were performed in solution, the solvent was the mixture solution of ethanol and DMF (*N*,*N*-dimethyl formamide) with the volume ratio of 1:1, and the concentration was 5×10^{-4} mol/L. As seen from the spectra, Calix[4]Br possesses the absorption peaks at about 287 and 241 nm, which is ascribed to the major π–π^* electronic transitions of aromatic ligands. Comparing the spectrum of Calix[4]Br–Si (B) with that of Calix[4]Br (A), we can see that an obvious blue shift (from 287 to 283 nm and from 241 to 237 nm) occurred, which suggests that the electron distribution of the modified ligand Calix[4]Br–Si has changed compared to free ligand Calix[4]Br due to the introduction of carbonyl group and that the TEPIC group has been successfully grafted to the ligand Calix[4]Br. From B to C, the corresponding red shift (from 283 to 289 nm and from 237 to 246 nm) is observed, which indicates that a more extensive π–π^* conjugating system is formed owing to the grafting reaction, and the Calix[4]Br groups are located on the surface of the mesoporous material MCM-41. The ultraviolet absorption spectra of Calix[4] (A), Calix[4]-Si (B), and Calix[4]-MCM-41 are shown in Fig. S2.

The ^{29}Si MAS NMR spectroscopy of the Calix[4]-functionalized mesoporous silica Calix[4]-MCM-41 is shown in Fig. 3. Distinct resonance peaks can be observed for the siloxane [Q^n=Si–(OSi)$_n$(OH)$_{4-n}$, n=2–4] and organosiloxane [T^m=R–Si–(OSi)$_m$(OH)$_{3-m}$, m=2, 3] species. The presence of T^3 and T^2 suggests that the organic group Calix[4]-Si has been grafted onto the wall of MCM-41. Meanwhile, the relative high intensity of organosiloxane T^3 NMR signal indicates that the incorporated Calix[4] groups are closely packed on the internal surface of the MCM-41 material via a primary strong linkage (three Si–O–Si covalent bonds).

3.2. *Rare earth (Eu^{3+}, Tb^{3+}) complexes covalently bonded to calixarene-functionalized mesoporous silica MCM-41*

Schemes 1 and S1 present the synthesis process and the predicted structure of the rare earth mesoporous hybrid materials *RE*-Calix[4]-MCM-41 and *RE*-Calix[4]Br-MCM-41, respectively. As we know, it is very difficult to prove the exact structure of this kind of non-crystalline hybrid materials and even it is hardly possible to solve the coordination behavior of rare earth ions. However it can be predicted the main composition and coordination effect according to the rare earth coordination chemistry principle and the configuration of the organic functional groups. The rare earth positive ions are Lewis hard acid so it is easy to coordinate with the hard base containing the oxygen and nitrogen atoms. Most of the rare earth complexes hold the polar covalent bonds, since the rare earth ions always make bonding through the 6*s*, 6*p*, and 5*d* electronic orbits, whose total amount is nine. Therefore, it is the most stable for the rare earth complex to exist with the coordination number of eight or nine. Furthermore, in the experiment we synthesize the material by adding the appropriate and accurate proportion of reagent into the system (RE^{3+}: Calix[4]-MCM-41=1:1, and RE^{3+}: Calix[4]Br-MCM-41=1: 2) to obtain the fixed model of rare earth complex. Furthermore, in view of the spatial steric hindrance effect, we predicted the optimum coordination structure for the hybrid materials. This prediction has also been confirmed by infrared spectra.

The FTIR spectra of pure MCM-41 and all obtained rare earth mesoporous hybrids are measured and are shown in Fig. 4. In the MCM-41 host material, the evident peaks appearing at 1000–1250 cm^{-1} are due to asymmetric Si–O stretching vibration modes (ν_{as}, Si–O), and the peak at 800 cm^{-1} can be attributed

to the symmetric Si–O stretching vibration (v_s, Si–O).The Si–O–Si bending vibration (δ, Si–O–Si) can also be observed at 468 cm^{-1}, and the band at 962 cm^{-1} is associated with silanol (Si–OH) stretching vibrations of surface groups [31]. In addition, the presence of hydroxyl can be clearly evidenced by the peak at 3465 cm^{-1}. Compared with MCM-41, the mesoporous hybrid materials *RE*-Calix[4]-MCM-41 and *RE*-Calix[4]Br-MCM-41 (*RE*=Eu, Tb) not only show the similar infrared absorption bands as the silica framework, but also the peaks at about 1558 cm^{-1} and peaks about 2927 and 2826 cm^{-1}, which are just the absorption bands of –CONH– and $-CH_2-$ group of modified organic ligand, indicating that organic ligands Calix[4] and Calix[4]Br have been grafted onto the wall of MCM-41.

The small-angle X-ray diffraction (SAXRD) patterns and nitrogen adsorption/desorption isotherms are popular and efficient methods to characterize highly ordered mesoporous material with hexagonal symmetry of the space group *P*6*mm*. The SAXRD patterns of a pure MCM-41(a) (which prepared according to Ref. [32]), Eu-Calix[4]-MCM-41 (b), Tb-Calix[4]-MCM-41 (c), Eu-Calix[4]Br-MCM-41 (d), and Tb-Calix[4]-MCM-41 (e) are shown in Fig. 5. The pure MCM-41 sample exhibits distinct Bragg peaks in the 2θ range of 1–6°, which can be indexed as (100), (110), and (200) reflections. The *d* value of the (100) reflection is 4.05 nm, and the lattice constant a=4.68 nm ($=2d_{100}/\sqrt{3}$). Upon functionalization of MCM-41 and subsequent inclusion of the rare earth complex, the characteristic reflections are still observed at about the same positions, suggesting that the long-range hexagonal symmetry of the mesoporous host is preserved. The attenuation of the X-ray peaks, especially after inclusion of the bulky rare earth complex, is not interpreted as a loss of crystallinity but rather to a reduction in the X-ray scattering contrast between the silica walls and pore-filling material [33]. In addition, the hexagonal mesostructure of Tb-Calix[4]-MCM-41 is further confirmed by TEM micrographs, which presents in Fig. 6. It shows the well regular hexagonal array of uniform channels, characteristic of mesoporous MCM-41 material, indicating that the mesostructure of Tb-Calix[4]-MCM-41 materials can substantially be conserved after the complexation process. The distance between the centers of the mesopores is estimated to be about 4 nm, which is in good agreement with the value determined from the corresponding XRD data (see Table 1).

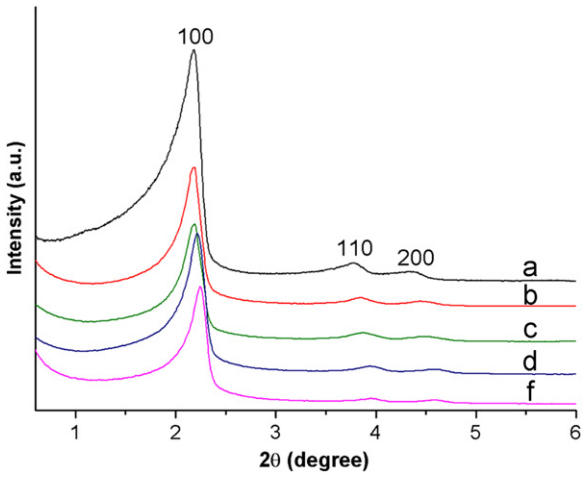

Fig. 5. SAXRD patterns of MCM-41 (a), Eu-Calix[4]-MCM-41 (b), Tb-Calix[4]-MCM-41 (c), Eu-Calix[4]Br-MCM-41 (d), and Tb-Calix[4]-MCM-41 (e).

In order to further investigate the channel structure of these materials, the characterization of the nitrogen adsorption–desorption is also carried out. The corresponding isotherms are presented in Fig. 7. They all exhibit the typical type IV isotherms with distinct H1-type hysteresis loops at low relative pressures according to the IUPAC classification [34,35], corresponding to the characteristic of mesoporous materials with highly uniform size distributions. The specific area and pore size have been calculated using Brunauer–Emmett–Teller (BET) and Barrett–Joyner–Halenda (BJH) methods, respectively. The structure data of all these mesoporous materials (BET surface area, total pore volume, and pore size, etc.) are summarized in Table 1. It is known from Table 1, the pure MCM-41 possesses very high S_{BET} of 1028 m^2/g, a large pore volume of 0.81 cm^3/g, and a BJH pore diameter of 3.13 nm, indicative of its potential application as a host in

Table 1
Structural parameters of MCM-41, *Ln*-Calix[4]-MCM-41 and *Ln*-Calix[4]Br-MCM-41 (*Ln*=Eu, Tb).[a]

Sample	d_{100} (nm)	a_0 (nm)	S_{BET} (m^2/g)	V (cm^3/g)	D (nm)	t (nm)
MCM-41	4.05	4.68	1028	0.81	3.13	1.55
Calix[4]-MCM-41	4.01	4.63	948	0.76	2.96	1.67
Eu-Calix[4]-MCM-41	4.03	4.65	902	0.73	2.84	1.81
Tb-Calix[4]-MCM-41	4.03	4.65	865	0.66	2.69	1.96
Eu-Calix[4]Br-MCM-41	3.99	4.61	846	0.74	3.06	1.55
Tb-Calix[4]Br-MCM-41	3.93	4.54	733	0.58	2.66	1.88

[a] d_{100} is the d(100) spacing, a_0 the cell parameter ($a_0=2d_{100}/\sqrt{3}$), S_{BET} the BET surface area, V the total pore volume, D_{BJH} the average pore diameter, and t the wall thickness, calculated by a_0-D.

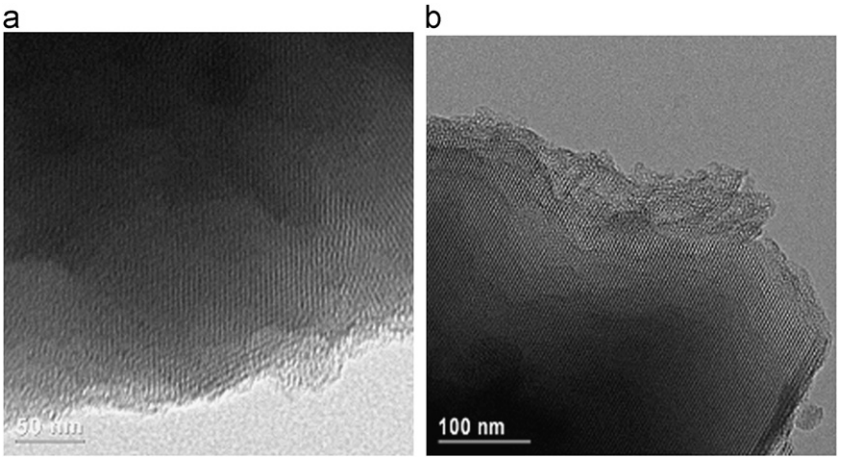

Fig. 6. TEM images of hybrid Tb-C[4]-MCM-41 material recorded along the [100] (a) and [110] (b) zone axes.

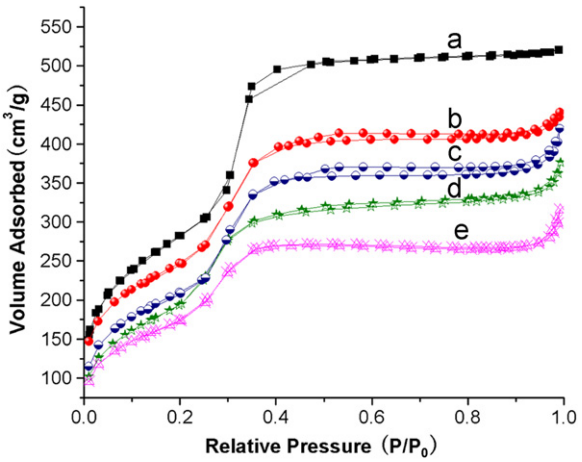

Fig. 7. N_2 adsorption–desoption isotherms for MCM-41 (a), Eu-Calix[4]-MCM-41 (b), Tb-Calix[4]-MCM-41 (c), Eu-Calix[4]Br-MCM-41 (d), and Tb-Calix[4]-MCM-41 (e).

luminescent materials. Upon functionalization of MCM-41 and subsequent inclusion of the rare earth complex, the specific area, pore size, and pore volume of these mesoporous hybrid materials are smaller in comparison with those of pure MCM-41, which may be due to presence of organic ligand on the pore surface and the co-surfactant effect of Calix[4]-Si (or Calix[4]Br–Si), which interacts with surfactant and reduces the diameter of the micelles [36].

3.2.1. *Antenna effects and luminescence*

The luminescence excitation of the resulting terbium and europium mesoporous hybrids are displayed in Figs. 8a and 9a, respectively. The excitation spectra are obtained by monitoring the emission of Tb^{3+} or Eu^{3+} ions at 613 or 545 nm. The excitation of terbium mesoporous hybrids shows a large broad band centered at about 308–314 nm, which are ascribed to the ligand-to-metal charge-transfer (CT) transition caused by interaction between the organic groups and the rare-earth ion [37]. No apparent *f–f* transitions could be observed in the spectra. The wide CT excitation bands will benefit the energy transfer and luminescence to terbium ions. Besides, the excitation spectrum of Tb-C[4]-MCM-41 shows a broader band range and a stronger intensity than those of Tb-C[4]Br-MCM-41, which indicates that Calix[4]-Si has a better energy match with Tb^{3+} than Calix[4]Br–Si. For europium mesoporous hybrids, the excitation are dominated by a broad band and a narrow peak centered at 393 nm, and the former band is attributed to the absorption of the precursor and the latter narrow peak is ascribed to the absorption of *f–f* electron transition of Eu^{3+}, which indicates that the energy transfer from organic ligand to Eu^{3+} ion is not very efficient. This may be explained by energy transfer degree. According to intramolecular energy transfer mechanism [38], the corresponding intramolecular transfer efficiency from the organic ligand to central rare earth ion mainly depends on the energy match between the triplet state energy of ligand and the resonant emissive energy level of the central RE^{3+} (17,250 cm^{-1} for Eu^{3+}, 20,500 cm^{-1} for Tb^{3+}). As reported in the literature [27], the lowest triple state energy of the organic ligand Calix[4]-Si and Calix[4]Br–Si are 22,880 cm^{-1} and 23,920 cm^{-1}, respectively. The energy differences between the triplet state energy of Calix[4]-Si (Calix[4]Br–Si) and the resonant emissive energy level of Eu^{3+} is 5630 cm^{-1} (6670 cm^{-1}), while the energy differences between the triplet state energy of C[4]-Si (C[4]Br–Si) and the resonant emissive energy level of Tb^{3+} is 2380 cm^{-1} (3420 cm^{-1}).

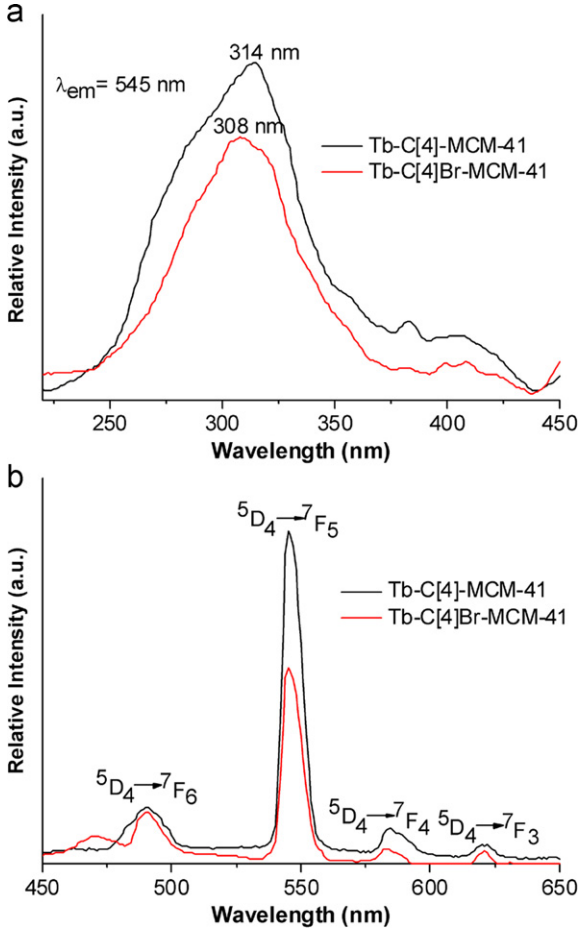

Fig. 8. Luminescent excitation (a) and emission (b) spectra of the mesoporous hybrid materials Eu-Calix[4]-MCM-41 and Eu-Calix[4]Br-MCM-41.

Thus, the triplet energy level of organic ligand (Calix[4]-Si and Calix[4]Br–Si) is more suitable for the luminescence of Tb^{3+} ions than that of Eu^{3+} ions.

As shown in Fig. 8b, upon excitation of the ligands' absorption band at 314 and 308 nm, respectively, the terbium mesoporous hybrids Tb-Calix[4]-MCM-41 and Tb-Calix[4]Br-MCM-41 exhibit the characteristic emission bands of Tb^{3+} ion centered at 490, 545, 585, and 620 nm, corresponding to the $^5D_4 \rightarrow {}^7F_J$ transitions (J=6, 5, 4, and 3, respectively). Furthermore, the low baseline indicates that the Si–O network absorption could be neglected, leaching of the photoactive molecules has been avoided and the effective energy transfer took place between the modified organic ligands and the chelated terbium ion. The mesoporous hybrid materials show relatively strong emission owing to the chemically covalently bonded molecular Si–O network structure between the complex and the mesoporous silica.

Fig. 9b displays typical photoluminescence spectra of the europium covalently bonded mesoporous hybrids. Narrow-width emission bands with maximum wavelengths at 575, 589, 613, 652, and 704 nm are recorded. These bands are related to the transition from the triplet-state energy level of Eu^{3+} to the different single-state levels and are assigned to the $^5D_0 \rightarrow {}^7F_1$, $^5D_0 \rightarrow {}^7F_2$, $^5D_0 \rightarrow {}^7F_3$, $^5D_0 \rightarrow {}^7F_4$, and $^5D_0 \rightarrow {}^7F_5$ transitions of Eu^{3+} ions, respectively. The energy transfer from the phenolic ligand to europium (III) is not perfect, as can be noticed by the residual ligand emission before 470 nm. This is not a surprise because the poor energy level match has been described in this paper previously. The introduction of Calix[4]arenes group into the into organically modified MCM-41 mesoporous host can provide the

strong absorption in the UV region, which produce energy transfer from the excited state of calixarene derived MCM-41 to the emitting level of the lanthanide ion (the so-called "antenna effect"). In order to prove this, we have also measured the emission spectra of Eu/Tb free Calix[4]-MCM-41 and Calix[4]Br-MCM-41 (see Fig. S3 in Supporting Information) Comparing Figs. S3, 8b, and 9b, it can be found that there exist the emission of Calix[4]-MCM-41 and Calix[4]Br-MCM-41 in Fig. 9b for Eu mesoporous hybrids (Eu-Calix[4]-MCM-41 and Eu-Calix[4]Br-MCM-41) while not in Fig. 8b for Tb mesoporous hybrids (Tb-Calix[4]-MCM-41 and Tb-Calix[4]Br-MCM-41). So it can be concluded that the energy transfer between Calix[4]-MCM-41 and Calix[4]Br-MCM-41 to Tb^{3+} are more effective than to Eu^{3+}. Among all emission peaks of the europium mesoporous hybrids, the most striking red fluorescence ($^5D_0 \rightarrow {}^7F_2$) of the induced electric dipole transition at about 613 nm are all stronger than the orange emission intensities of magnetic dipole transition of $^5D_0 \rightarrow {}^7F_1$ at about 588 nm, which indicates a Eu^{3+} site in an environment without inversion symmetry [39]. As we know, the intensity ratio of $^5D_0 \rightarrow {}^7F_2$ to $^5D_0 \rightarrow {}^7F_1$ is sensitive to the symmetry around Eu^{3+} ion and gives valuable information about the chemical microenvironment change of anions coordinating the Eu^{3+} ion [40]. When the I_{02}/I_{01} value is higher, the Eu^{3+} ion occupies a site of lower symmetry without an inversion center. The I_{02}/I_{01} value for Eu-C[4]-MCM-41 and Eu-C[4]Br-MCM-41 are 3.68 and 1.97, respectively. This indicates that the Eu^{3+} site is situated in an environment without inversion symmetry.

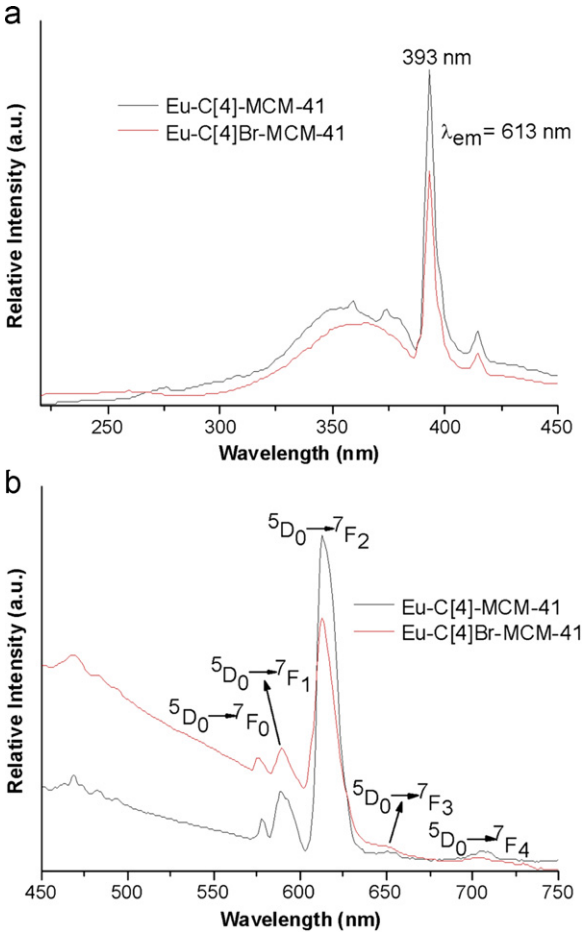

Fig. 9. Luminescent excitation (a) and emission (b) spectra of the mesoporous hybrid materials Tb-Calix[4]-MCM-41 and Tb-Calix[4]Br-MCM-41.

3.2.2. Luminescence decay times (τ) and emission quantum efficiency (η)

In order to further discuss the photophysical properties of the resulting mesoporou materials, the typical decay curves of the eurpium and terpium mesoporous hybrid materials are measured, and they can be described as a single exponential ($\ln(S_{(t)}/S_0) = -k_1 t = -t/\tau$), indicating that all Eu^{3+} and Tb^{3+}ions occupy the same average coordination environment. The resulting lifetime data of rare earth mesoporous hybrid materials are given in Table 2. It is found that the terbium mesoporous hybrids Tb-Calix[4]-MCM-41 and Tb-Calix[4]Br-MCM-41 present longer luminescent lifetimes than the europium mesoporous hybrids Eu-Calix[4]-MCM-41 and Eu-Calix[4]Br-MCM-41, suggesting that both Calix[4]Si and Calix[4]-Br–Si are more suitable for the luminescence of Tb^{3+} than that for Eu^{3+}.Therefore, the luminescent lifetime data for this rare earth covalently bonded mesopoeous hybrids correspond to the above analyses from the phosphorescence spectrum.

Furthermore, we selectively determined the emission quantum efficiencies of the $^5D_0$ excited state of the europium ion for Eu^{3+} mesoporous hybrids on the basis of the emission spectra and lifetimes of the $^5D_0$ emitting level. Assuming that only radiative and non-radiative processes are essentially involved in the depopulation of the $^5D_0$ state, radiative and non-radiative processes influence the experimental luminescence lifetime by the equation

$$\tau_{exp} = (A_r + A_{nr})^{-1} \quad (1)$$

Here, A_r and A_{nr} are radiative and non-radiative transition rates, respectively. A_r can be obtained by summing over the radiative rates A_{0J} for each $^5D_0 \rightarrow {}^7F_J$ (J=0–4) transitions.

The quantum efficiency of the luminescence step, η expresses how well the radiative processes (characterized by rate constant A_r) compete with non-radiative processes (overall rate constant A_{nr}):

$$\eta = A_r/(A_r + A_{nr}) \quad (2)$$

According to Refs. [41,42], the quantum efficiencies of the two different europium mesoporous hybrid materials can be determined, as shown in Table 2. From the equation of η, it can be seen that the value η mainly depends on the values of two factors: one is lifetime and the other is intensity ratio I_{02}/I_{01}. Since the transitions $^5D_0 \rightarrow {}^7F_1$ and $^5D_0 \rightarrow {}^7F_2$ are primary among all transitions, the ratio value of I_{02}/I_{01} has the most important influence on A_J. Even if the lifetime of Eu-Calix[4]Br-MCM-41 (315.8 μs) is

Table 2
Luminescence data of the mesoporous hybrid materials.

Hybrids	I_{02}/I_{01}	τ (μs)[a,b]	$1/\tau^-$ (s^{-1})	A_r (s^{-1})	A_{nr} (s^{-1})	η (%)	Ω_2 (10^{-20} cm^2)	Ω_4 (10^{-20} cm^2)
Eu-Calix[4]-MCM-41	3.68	277.1[a]	3609	320.1	3288.9	8.8	5.56	1.53
Eu-Calix[4]Br-MCM-41	1.97	315.8[a]	3167	229.1	3013.9	7.2	2.98	0.87
Tb-Calix[4]-MCM-41		504.2[b]						
Tb-Calix[4]Br-MCM-41		458.0[b]						

[a] For the $^5D_0 \rightarrow {}^7F_2$ transition of Eu^{3+}.
[b] For the $^5D_4 \rightarrow {}^7F_5$ transition of Tb^{3+}.

slightly longer than that of Eu-Calix[4]-MCM-41 (277.1 μs), but due to that the ratio of I_{02}/I_{01} of Eu-C[4]-MCM-41 (3.68) is almost two times as that of Eu-C[4]Br-MCM-41 (1.97), the quantum efficiency of Eu-Calix[4]-MCM-41 is larger than that of Eu-Calix[4]Br-MCM-41. This indicates that the energy transfer efficiencies from Calix[4]-Si to Eu^{3+} is higher than that of Calix[4]Br–Si to Eu^{3+}, which is in agreement with the energy match between Calix[4]-Si (Calix[4]-Br–Si) and Eu^{3+} ion. The energy difference $\Delta E(Tr–Eu^{3+})$ of Calix[4]-Br–Si (6670 cm^{-1}) is worse than that of Calix[4]-Si (5630 cm^{-1}) and is so large that it decreases the energy transfer from the triplet state of Calix[4]-Br–Si to Eu^{3+}, so the energy match between Calix[4]-Br–Si and Eu^{3+} is less suitable than that between Calix[4]-Si and Eu^{3+}. Ulteriorly, the steric exclusion effect could not be excluded to be responsible to poor luminescent properties of Eu-Calix[4]Br-MCM-41. In addition, compared with the rare earth hybrids Eu-Calix[4]-Si (3.4%) and Eu-Calix[4]-Br–Si (6.5%) reported in the literature [23], the quantum efficiency of corresponding rare earth mesoporous hybrids Eu-Calix[4]-MCM-41 (8.8%) and Eu-Calix[4]Br-MCM-41 (7.2%) are higher, which shows that MCM-41 is an excellent host for the rare earth calix complex.

To study the coordination environment surrounding rare earth ions, especially the influence caused by vibrations of water molecules, according to Horrocks' previous research [43,44], the probable number of coordinated water molecules (n_w) can be determined as following equation:

$$n_w = 1.05A_{nr} \quad (3)$$

Based on the results, the coordination number of water molecules (Eu containing hybrid materials) can be estimated to be four. The coordinated water molecules produce the severe vibration of hydroxyl group, resulting in the large non-radiative transition and decreasing the luminescent efficiency.

3.3. Thermogravimetric analysis (TGA)

To investigate the thermal stability of all obtained hybrids, the thermogravimetric analysis (TGA) are performed at a heating rate of 15.0 °C/min under nitrogen atomosphere. TG analysis shows that the thermal decomposition behavior of all these mesoporous hybrids is similar, so we present the thermogravimetric weight loss curve (TG) and derivative weight loss (DTG) curve of mesoporous hybrids Eu-Calix[4]Br-MCM-41 as an example (see Fig. 10). From the TG curve we can see that the decomposition of the hybrid Eu-Calix[4]Br-MCM-41 undergoes in three stages. The first stage between 30 and 217 °C with a mass loss of 2.3% is due to the physically absorbed water and residual solvent, without any decomposition of the chemical bonds. This is followed by a weight loss (approximately 13.8%) between 217 and 423 °C, which are ascribed to the decomposition of the incompletely removed surfactant. The third weight loss (approximately 13.1%) between 423 and 780 °C is attributed to the decomposition of europium complex, corresponding to a main weight loss peak centered at 524 °C. In addition, the weight loss peak of the hybrid Eu-Calix[4]Br–Si is reported to be 324 °C, indicating that the thermal stability of the rare earth complex is enhanced as it is covalently introduced into the mesoporous matrix. Furthermore, the weight loss peak of pure complex Eu–C[4]Br is 347 °C (see Fig. S4), which further prove the above conclusion.

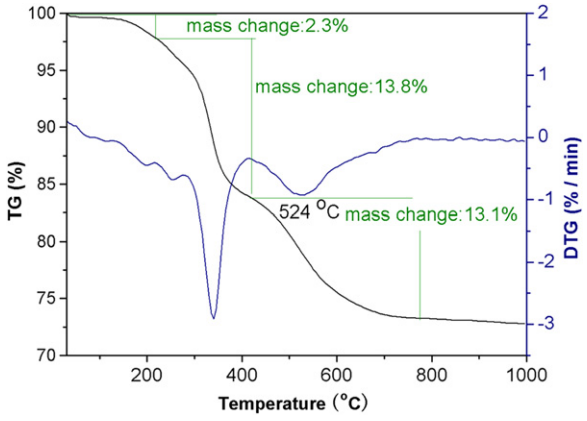

Fig. 10. TG and DTG curves of mesoporous hybrid material Eu-Calix[4]Br-MCM-41.

4. Conclusions

In summary, we obtained the organic–inorganic mesoporous luminescent hybrid materials by linking the ternary rare earth (Eu^{3+}, Tb^{3+}) complexes to the functionalized ordered mesoporous MCM-41 with the modified calix[4]arene derivatives (Calix[4]-Si and Calix[4]Br–Si) via co-condensation of tetraethoxysilane in the presence of cetyltrimethylammonium bromide (CTAB) surfactant as a template. The precursors are synthesized by grafting Calix[4] and Calix[4]Br to the coupling agent TEPIC, respectively. The synthesis of Calix[4]-MCM-41 and Calix[4]Br-MCM-41 provides a convenient approach of tailoring the surface properties of mesoporous silicates by organic functionalization, and the resulting material *RE*-Calix[4]-MCM-41 and *RE*-Calix[4]Br-MCM-41 all retain the ordered mesoporous structures. Further investigation into the luminescence properties of all the resulting mesoporous hybrid materials show that the characteristic luminescence of the corresponding rare earth ions (RE^{3+}) through the intramolecular energy transfers from the modified ligand to the rare earth ions. Furthermore, the hybrid Tb-Calix[4]-MCM-41 and Eu-Calix[4]-MCM-41 present stronger luminescence intensity and longer lifetime than corresponding hybrid Tb-Calix[4]Br-MCM-41 and Eu-Calix[4]-MCM-41. In addition, it is rather meaningful that macrocylic calix[4]arene derivative could be initially introduced in MCM-41 through covalent bonds that may heavily affect the photostability or thermal stability of rare earth-calix[4]arene complexes.

Acknowledgment

This work is supported by the National Natural Science Foundation of China (20971100) and Program for New Century Excellent Talents in University (NCET-08-0398) and the Developing Science Funds of Tongji University.

Appendix A. Supplementary material

Supplementary data associated with this article can be found in the online version at doi:10.1016/j.jssc.2011.07.040.

References

[1] K.N. Koh, K. Araki, A. Ikeda, H. Otsuka, S. Shinkai, J. Am. Chem. Soc. 118 (1996) 755–758.
[2] L. Wang, X.F. Shi, P.J. Jia, Y. Yang, J. Polym. Sci. A: Polym. Chem. 42 (2004) 6259–6266.
[3] P.D. Beer, F. Szemes, P. Passaniti, M. Maestri, Inorg. Chem. 13 (2004) 3965–3975.
[4] G. Blasse, B.C. Grabmaier, Luminescent Materials, Springer, Berlin, 1994.
[5] Z. Asfari, V. Böhmer, J. Harrowfield, J. Vicens, Calixarenes, Dordrecht, Holland, 2001.
[6] X.M. Guo, H.D. Guo, L.S. Fu, L.D. Carlos, R.A.S. Ferreira, L.N. Sun, R.P. Deng, H.J. Zhang, J. Phys. Chem. C 113 (2003) 12538–12545.

[7] L.D. Carlos, R.A.S. Ferreira, V.D. Bermudez, S.J.L. Ribeiro, Adv. Mater. 21 (2009) 509–534.
[8] K. Binnemans, Chem. Rev. 109 (2009) 4283–4374.
[9] M.P. Lowe, D. Parker, O. Reany, S. Aime, M. Botta, G. Castellano, E. Gianolio, R. Pagliarin, J. Am. Chem. Soc. 123 (2001) 7601–7609.
[10] J.L. Liu, B. Yan, J. Phys. Chem. C 112 (2008) 14168–14178.
[11] J. Kido, Y. Okamoto, Chem. Rev. 102 (2002) 2357–2368.
[12] M.D. McGehee, T. Bergstedt, C. Zhang, A.P. Saab, M.B. O'Regan, G.C. Bazan, V.I. Srdanov, A.J. Heeger, Adv. Mater. 17 (1999) 1349–1354.
[13] K. Binnemans, D. Moors, J. Mater. Chem. 12 (2002) 3374–3376.
[14] Y.J. Li, B. Yan, Y. Li, Chem. Asian J. 5 (2010) 1642–1650.
[15] J. Choi, R. Tamaki, S.G. Kim, R.M. Laine, Chem. Mater. 15 (2003) 3365–3375.
[16] X.M. Guo, H.D. Guo, L.S. Fu, H.J. Zhang, L.D. Carlos, R.P. Deng, J.B. Yu, J. Photochem. Photobiol. A Chem. 200 (2008) 318–324.
[17] F.Y. Liu, L.D. Carlos, R.A.S. Ferreira, J. Rocha, M.C. Gaudino, M. Robitzer, F. Quignard, Biomacromolecules 9 (2009) 1945–1950.
[18] A. Fernandes, J. Dexpert-Ghys, A. Gleizes, A. Galarneau, D. Brunel, Microporous Mesoporous Mater. 83 (2005) 35–46.
[19] D. Chandra, T. Yokoi, T. Tatsumi, A. Bhaumik, Chem. Mater. 19 (2007) 5347–5354.
[20] D. Chandra, S.K. Das, A. Bhaumik, Microporous Mesoporous Mater. 128 (2010) 34–40.
[21] Q.H. Zuo, B. Li, L.M. Zhang, Y.H. Wang, Y.H. Liu, J. Zhang, Y. Chen, L.F. Guo, J. Solid State Chem. 183 (2010) 1715–1720.
[22] C. Zhang, S.Y. Guang, H.Y. Xu, J. Solid State Chem. 183 (2010) 1409–1415.
[23] C.T. Kresge, M.E. Leonowicz, W.J. Roth, J.C. Vartuli, J.S. Beck, Nature 359 (1992) 710–712.
[24] B.L. Su, X.C. Mab, F. Xu, L.H. Chen, Z.Y. Fu, N. Moniotte, S. Ben Maamar, R. Lamartine, F. Vocanson, J. Colloid Interface Sci. 360 (2011) 86–92.
[25] J. Feng, S.Y. Song, W.Q. Fan, L.N. Sun, X.M. Guo, C.Y. Peng, J.B. Yu, Y.N. Yu, H.J. Zhang, Microporous Mesoporous Mater. 117 (2009) 278–284.
[26] L.N. Sun, H.J. Zhang, C.Y. Peng, J.B. Yu, Q.G. Meng, L.S. Fu, F.Y. Liu, X.M. Guo, J. Phys. Chem. B 110 (2006) 7249–7258.
[27] Y. Li, B. Yan, Y.J. Li, Microporous Mesoporous Mater. 128 (2010) 62–70.
[28] B. Yan, Y. Li, B. Zhou, Microporous Mesoporous Mater. 120 (2009) 317–324.
[29] H.F. Lu, B. Yan, J.L. Liu, Inorg. Chem. 48 (2009) 3966–3975.
[30] A.C. Franville, R. Mahiou, Z. Zambon, J.C. Cousseins, Solid State Sci. 3 (2001) 211–222.
[31] M.V. Landau, S.P. Parkey, M. Herskowitz, O. Regev, S. Pevzner, T. Sen, Z. Luz, Microporous Mesoporous Mater. 33 (1993) 149–163.
[32] J. Hukkamäki, S. Suvanto, M. Suvanto, T.T. Pakkanen, Langmuir 20 (2004) 10288–10295.
[33] S. Gago, Y.M. Zhang, A.M. Santos, K. Köhler, F.E. Kühn, J.A. Fernandes, M. Pillinger, A.A. Valente, T.M. Santos, P.J.A. Ribeiro-Claro, I.S. Gonçalves, Microporous Mesoporous Mater. 76 (2004) 131–136.
[34] M.H. Lim, A. Stein, Chem. Mater. 11 (1999) 3285–3295.
[35] W.H. Zhang, X.B. Lu, J.H. Xiu, Z.L. Hua, L.X. Zhang, M. Robertson, J.L. Shi, D.S. Yan, J.D. Holmes, Adv. Funct. Mater. 14 (2004) 544–552.
[36] Q.Y. Hu, J.E. Hampsey, N. Jiang, C.J. Li, Y.F. Lu, Chem. Mater. 17 (2005) 1561–1569.
[37] K. Binnemans, P. Lenaerts, K. Driesen, C. Gorller-Walrand, J. Mater. Chem. 14 (2004) 191–195.
[38] Q.M. Wang, B. Yan, X.H. Zhang, J. Photochem. Photobiol. A Chem. 174 (2005) 119–124.
[39] Y. Hasegawa, M. Yamamuro, Y. Wada, N. Kanehisa, Y. Kai, S. Yanagida, J. Phys. Chem. A 107 (2003) 1697–1702.
[40] A.F. Kirby, D. Foster, F.S. Richardson, Chem. Phys. Lett. 95 (1983) 507–512.
[41] E.E.S. Teotonio, J.G.P. Espynola, H.F. Brito, O.L. Malta, S.F. Oliveria D.L.A. de Foria, C.M.S. Izumi, Polyhedron 21 (2002) 1837–1844.
[42] M.H.V. Werts, R.T.F. Jukes, J.W. Verhoeven, Phys. Chem. Chem. Phys. 4 (2002) 1542–1548.
[43] W.DeW Horrocks, D.R. Sudnick, J. Am. Chem. Soc. 101 (1979) 334–340.
[44] W.DeW Horrocks, D.R. Sudnick, Acc. Chem. Res. 14 (1981) 384–392.